

PDF hosted at the Radboud Repository of the Radboud University Nijmegen

The following full text is a preprint version which may differ from the publisher's version.

For additional information about this publication click this link.

<http://hdl.handle.net/2066/28371>

Please be advised that this information was generated on 2018-07-19 and may be subject to change.

Measurement of the Weak Charged Current Structure in Semileptonic b-Hadron Decays at the Z Peak

The L3 Collaboration

Abstract

The neutrino energy spectrum in semileptonic b-hadron decays with identified energetic electrons and muons has been measured. The observed relative energy sharing between the neutrino and the charged lepton is found to be well described with a W^\pm polarization obtained from a free b-quark decay model with a $(V-A)\times(V-A)$ decay structure.

The alternative of a $(V+A)\times(V-A)$ decay structure is excluded with a significance of more than 6 standard deviations. The possibility that hadronic corrections to the b-hadron decay destroy any W^\pm polarization is disfavored by more than 3 standard deviations.

(Submitted to Physics Letters B)

1 Introduction

Semileptonic b -quark decays, $b \rightarrow q\ell\nu$, are usually studied with energetic electrons, muons and charmed hadrons [1]. These decays can also be studied using neutrinos, which can be measured indirectly from the missing energy associated with the b -quark decay.

After quark masses are adjusted, a good description of the observed charged lepton spectrum from semileptonic b -hadron decays can be obtained with the free b -quark model [2]. Within this model the energy spectra and the relative energy sharing between the charged lepton and the neutrino depend on the structure of the weak charged current, the virtual W^\pm . Assuming a similarity between the muon decay and the b -quark decay, parity violation effects due to the $(V-A)\times(V-A)$ decay structure are predicted for semileptonic b -quark decays. According to this picture, the energy spectrum of the charged lepton is expected to be slightly harder than the neutrino energy spectrum. Gronau and Wakaizumi have pointed out that no strong experimental justification exists which can exclude the possibility of a $(V+A)\times(V-A)$ b -quark decay structure [3].

Recently, a measurement of the relative energy sharing between the charged lepton and the neutrino was proposed as a way to measure the parity violation strength in b -hadron decays [4]. It was shown that the inclusive charged lepton spectrum can be described by any model, if the different exclusive b -hadron decay modes and the mechanism of the b -hadron formation at the Z peak are chosen appropriately within the experimental bounds. However, once the charged lepton spectrum is described, a definite prediction for the neutrino energy spectrum exists within the given model. Thus, a measurement of the relative energy sharing between the charged lepton and the neutrino is sensitive to the parity violation in semileptonic b -hadron decays. In detail it was found that such a measurement should allow a $(V-A)\times(V-A)$, the exotic $(V+A)\times(V-A)$ and the kaon-like $V\times(V-A)$ decay structures to be distinguished.

A measurement of the neutrino energy spectrum in tagged semileptonic b -hadron decays is described. The neutrino energy is obtained from the difference between the beam energy and the observed jet energy $E_\nu \approx E_{beam} - E_{jet}$. The analysis is restricted to two-jet events as this expression for the neutrino energy is not valid for hard three-jet events.

2 The L3 Detector and the Hadronic Event Selection

The L3 detector consists of a central tracking chamber, a high resolution electromagnetic calorimeter composed of BGO crystals, a cylindrical array of scintillation counters, a uranium and brass hadron calorimeter with proportional wire chamber readout, and a precise muon spectrometer. These subdetectors are installed in a 12 m diameter solenoid which provides a uniform magnetic field of 0.5 T along the beam direction. A detailed description of the L3 detector can be found elsewhere [5].

Approximately one million hadronic Z decays, collected during the 1991 and 1992 data taking periods, were selected using the criteria described in reference 6. For this study only the events with a center-of-mass energy within 0.5 GeV of the Z mass have been analyzed. To

ensure that the jets are well measured, the missing energy analysis is restricted to the hermetic barrel region of the experiment. In detail, the following additional criteria are used:

- The visible energy in each hemisphere, defined with respect to the thrust axis of the event, has to be larger than 10% of the beam energy. The polar angle, θ_H , of the momentum vector sum of all calorimeter clusters associated with each hemisphere has to fulfill the condition $|\cos \theta_H| < 0.7$. For the hemisphere which is used for the neutrino measurement the condition $|\cos \theta_H| < 0.65$ is required.
- To remove events with three hard isolated jets, it is required that the reconstructed invariant mass per hemisphere is less than 25 GeV and that the energy sum of all calorimeter clusters with $|\cos \theta| > 0.74$ is smaller than 5 GeV.
- To remove events with hard initial state radiation and remaining background from two-photon processes, events with a visible energy smaller than 70% of the center-of-mass energy have to fulfill the condition that the missing transverse energy of the event is larger than 50% of the beam energy or that it is larger than the missing longitudinal energy.
- To remove remaining background from Z decays into $\tau^+\tau^-(\gamma)$, the number of charged tracks in the event has to be larger than four and at least three tracks, each with a transverse momentum with respect to the beam of more than 150 MeV and a distance of closest approach to the event vertex smaller than 1 mm, are found in one hemisphere.

With these criteria about 350k hadronic events are selected in the data and 611k events in the Monte Carlo. The fraction of background events from $\tau^+\tau^-$ pairs and two-photon events are found to be negligible.

The hadronic Monte Carlo events are simulated using JETSET [7] and a GEANT based description of the L3 experiment [8]. Weak decays of c and b-hadrons are simulated such that the measured inclusive charged lepton spectra and the branching ratios for charm and beauty decays, [9–11], are found to be reproduced. In detail, a $(V+A)\times(V-A)$ structure¹ is used for semileptonic charm decays, $c\rightarrow X\ell\nu$, with the exclusive branching ratios $D^0\rightarrow K(K^*)\ell\nu$ of 3.8% (2.4%) for the three-body decays and 0.8% for multibody decays. The exclusive branching ratios for the corresponding D^+ decays are 9.8% (6.2%) and 2% respectively. For semileptonic b-hadron decays, a $(V-A)\times(V-A)$ structure with inclusive branching ratios, $b\rightarrow X\ell\nu$, of 10.45% for electrons and muons and 2.5% for τ 's is used. The different charm hadrons, X, are simulated with semileptonic branching ratios for $B\rightarrow D, D^*, D^{**}\ell\nu$ of 2.0%, 5.3% and 3.0% respectively. The semileptonic $b\rightarrow u\ell\nu$ decays have a branching ratio of 0.15%. Furthermore, weak b-meson decays into hadronic final states are generated without polarization and the c and b-baryon states are assumed to be unpolarized. For this study the energy spectra of the weakly decaying b-hadrons (B_d, B_u, B_s and Λ_b) are simulated with the Peterson function [12] with an average energy of 72% of the beam energy. As will be shown below, a good agreement between the observed charged lepton spectra in the data and in the simulation is obtained.

¹For the decays $D\rightarrow K\ell\nu$ a $V\times(V-A)$ structure is expected, resulting in a slightly softer neutrino energy spectrum.

3 The Jet Energy Measurement

To measure the missing energy associated with jets as accurately as possible, a special method has been developed to obtain the jet energy. The method uses the fact that electromagnetic showering particles (photons and electrons) are measured very accurately in the BGO calorimeter. The energy of hadronic showering particles is measured with a non-linear energy response, the e/π ratio, from a combination of the energy deposits in the BGO and hadron calorimeters.

The visible energy of a jet is calculated using the energy deposits from its associated clusters in the BGO and hadron calorimeters, as well as the measured muon momenta obtained from the muon system. For this analysis, all clusters found within a geometrical cone of 30° around the jet axis, starting from the most energetic cluster in the calorimeter, are combined to form a jet. The event is then divided into two hemispheres using the thrust axis. If more than one jet is found per hemisphere, pairs of jets are further combined into a single jet if their invariant mass is smaller than 25 GeV.

The algorithm used to obtain the best jet energy measurement proceeds as follows. The BGO clusters are separated into electromagnetic and hadronic showers, using the shower shape in the BGO. On average, an energy of about 10 GeV per hemisphere is found in electromagnetic showers. In addition, an average energy deposit of about 25 GeV in the BGO and the hadron calorimeters, is associated with hadronic showering particles. Using jets which contain different amounts of well measured electromagnetic energy, correction factors for the e/π ratio of hadronic showers are determined from the energy deposits and the requirement that the energy sum per hemisphere from electromagnetic showers, hadronic showers and muons should be independent of the fraction of well measured electromagnetic energy.

In order to measure the neutrino energy scale as accurately as possible, the usual jet energy calibration method, which uses the beam energy or the center of mass energy as a constraint, cannot be used. Instead, the Monte Carlo is used to define the energy scale. It is required that the average missing energy of jets in Monte Carlo events with semileptonic b-hadron decays equals the average neutrino energy. Using this condition, the absolute energy scale for the calorimeters are defined and used for all Monte Carlo jets.

The calibration constants for the absolute energy scale in the data are determined such that the energy response to high energy jets, which contain essentially no missing energy due to neutrinos, is equivalent to the high energy Monte Carlo jets. This energy scale is obtained from a Gaussian fit to the jet energy distribution between 40 GeV and 65 GeV, a region which is largely independent of missing energy due to neutrinos. Using this procedure, a mean jet energy of 43.96 GeV is obtained for the Monte Carlo events and 43.97 GeV for the data. Separating the data into the 1991 and 1992 data samples, the mean energy values obtained from the fit are found to be 43.94 GeV (1991), 43.98 GeV (1992).

The jet energy distribution for the Monte Carlo and for the data sample with the fitted curve are shown in Figure 1. The resolution in the data for jet energies between 40 and 60 GeV is well described by a Gaussian distribution with a sigma of 4.2 GeV. The resolution in the Monte Carlo is found to be 4.6 GeV, roughly 10% larger than in the data. For lower visible energies the distributions are not Gaussian because of energetic neutrinos and detector gaps.

4 The Neutrino Energy Spectrum

Semileptonic b-hadron decays are selected using events with inclusive high momentum electron or muon candidates which have a measured energy of less than 35 GeV. Electrons are identified using the electromagnetic shower shape in the BGO calorimeter and requiring a good geometrical matching of a charged track with this electromagnetic cluster. A total of 5366 inclusive electrons with an energy above 3 GeV and a transverse momentum, p_t , of more than 1.4 GeV to the nearest jet is selected. The jet direction is estimated from all associated clusters excluding the charged lepton. Muons are identified using tracks reconstructed in the muon chambers which point to the event vertex. A total of 9746 inclusive muons with a momentum above 4 GeV and a p_t above 1.4 GeV are found.

The observed energy spectra for electrons and muons and their associated neutrinos in the data and the Monte Carlo are shown in Figures 2 and 3 respectively. The corresponding neutrino energy spectra are obtained from the missing energy of the associated jet, using the difference between the beam energy and the jet energy, which includes the charged lepton. The neutrino energy spectra for the ν_e and ν_μ candidates are shown in Figures 2b and 3b. The expected Monte Carlo spectra from semileptonic b-hadron decays with a $(V-A)\times(V-A)$ decay structure are also shown in Figures 2 and 3. The p and p_t spectra for the charged leptons are found to be described by the Monte Carlo. Discrepancies seen for small charged lepton energies and for negative neutrino energies are due to uncertainties in the efficiency to identify low energy electrons and muons, the background and the different jet energy resolution in the simulation.

The systematic errors are found to be the limiting factor in the interpretation of the measured neutrino energy spectra. The dominant systematic error contributions arise from the uncertainties in the jet energy calibration, the background from misidentified leptons and from the uncertainties in the Monte Carlo description of the charged lepton spectra.

The quality of the calibration for different quark flavors, has been studied using subsamples of events which are enriched in either light quark-flavor (u, d, s and c) or in b-flavor primary quarks. These subsamples are selected using the impact parameter distribution of charged tracks, high-energy hadrons or energetic leptons:

- Sample Ia is selected with the requirement that a high $x(= E_i/E_{beam})$ particle i is found in at least one hemisphere. It is required that either a high momentum track with a momentum above 60% of the beam energy and an associated calorimeter cluster of more than 50% of the beam energy, or that an energetic π^0 candidate with an energy above 50% of the beam energy is found in one hemisphere. With the additional requirement that no electron or muon candidates are found in these events, the remaining b-fraction is determined to be 7%. The reconstructed jet energy distribution in the hemisphere opposite to the one which contains the high x particle defines this light quark-flavor enriched event sample.
- Sample Ib is obtained from events, which have a negative reconstructed decay distance between the two hemispheres. The decay distance is calculated per hemisphere using the average decay length of high p_t tracks. With the requirement that no electron or muon

candidate is found in the event, the fraction of b–flavor events in this light quark–flavor sample is estimated to be 8%.

- Sample IIa is selected with the requirement that the estimated decay distance between the two hemispheres is larger than 3.5 mm; the fraction of $b\bar{b}$ events is determined to be about 61%.
- Sample IIb has a $b\bar{b}$ fraction of 80% and is obtained from the events which contain an energetic electron or muon candidate, selected with the criteria described above, in one jet. The reconstructed energy distribution in the jet opposite to the one containing the charged lepton is used for the comparison between the data and the Monte Carlo.

The observed mean energy and r.m.s. (σ) per jet, obtained from a Gaussian fit between 40 GeV and 65 GeV, for these b–flavor depleted and enriched event samples in the data and in the Monte Carlo are given in Table 1.

| Event Sample | Data | | Monte Carlo | | |
|--------------|---------------------------------|----------------|---------------------------------|----------------|------------|
| | $\langle E_{jet} \rangle$ [GeV] | σ [GeV] | $\langle E_{jet} \rangle$ [GeV] | σ [GeV] | b–fraction |
| Ia | 44.46 ± 0.03 | 4.1 | 44.49 ± 0.03 | 4.5 | 7% |
| Ib | 44.19 ± 0.01 | 4.1 | 44.23 ± 0.01 | 4.5 | 8% |
| IIa | 43.65 ± 0.03 | 4.2 | 43.49 ± 0.02 | 4.6 | 61% |
| IIb | 43.31 ± 0.05 | 4.3 | 43.18 ± 0.04 | 4.7 | 80% |

Table 1: The mean jet energies with their statistical errors and the r.m.s. obtained from Gaussian fits between 40 and 65 GeV to the visible energy spectrum per hemisphere. Event samples Ia and Ib are light quark–flavor enriched and IIa and IIb are b–flavor enriched.

The overall distributions of the visible energy per hemisphere for the different flavor dependent selections are found to be well described by the Monte Carlo simulation. For visible energies below 30 GeV, the non–Gaussian tails in the light quark–flavor samples are about 10% larger in the data than in the simulation. The resolutions obtained from Gaussian fits between 40 and 65 GeV for the four subsamples are between 4.1 GeV and 4.3 GeV for the data and between 4.5 GeV and 4.7 GeV for the Monte Carlo.

The mean energy values obtained from the fits to the light quark–flavor enriched event samples in the data are 30 to 40 MeV lower than the ones from the Monte Carlo. The mean energy values for the b–enriched sample IIa in the data shows a 160 ± 40 MeV higher value than in the Monte Carlo. For sample IIb, which has a higher b–purity, the discrepancy between the data and the Monte Carlo is found to be 130 ± 60 MeV. Uncertainties in the charm energy spectra from hadronic b–decays and the simulation of the neutrino energy spectra from semileptonic cascade charm decays have been studied as a possible origin of the observed difference between the data and the Monte Carlo. These uncertainties might explain up to 100 MeV of the observed difference for the mean energy value in the data and the Monte Carlo simulation for the b–flavor enriched event samples. As the reason for the difference between the data and the Monte Carlo is not well understood, a discrepancy of 150 MeV between the data and the Monte Carlo

from the b-flavor enriched samples is used as an estimate for the systematic error of the energy calibration.

The predicted charged lepton and neutrino energy spectra are correlated with the purity of the tagged semileptonic b-decay candidates. These depend on the semileptonic branching ratio of b-hadrons and on background contributions. According to the Monte Carlo, the electron sample consists of 75% identified $b \rightarrow X e \nu_e$ decays; 5% of the leptons originate from semileptonic cascade charm decays $b \rightarrow c \rightarrow X e \nu_e$; 5% are background from $b\bar{b}$ events and 15% from charm and light quark-flavor events. The corresponding numbers for the inclusive muon sample are 64% identified $b \rightarrow X \mu \nu_\mu$ decays, 9% $b \rightarrow c \rightarrow X \mu \nu_\mu$ decays, 5% background in $b\bar{b}$ events and 22% background from charm and light quark-flavor events.

From a variation of the assumed semileptonic b- and c-branching ratios in the Monte Carlo according to the errors given in [9], the total relative uncertainty for the purity of identified semileptonic b-hadron decays is determined to be less than $\pm 5\%$. This corresponds to an estimated semileptonic b-hadron fraction for the electron sample of $75 \pm 4\%$ and for the muon sample of $64 \pm 3\%$. A change of the assumed purity from 75% to 79% would increase the predicted average neutrino energy by 150 MeV and would decrease the average electron energy by 30 MeV. For the muons, a variation of the purity from 64% to 67% would increase the average predicted neutrino energy by 120 MeV and increases the average muon energy by 50 MeV. The estimated background contributions have also been studied using independent subsamples of charged lepton candidates which are found in the light flavor and b-flavor enriched lifetime event samples Ia and IIa. As a result one finds, with small statistical significance, that the estimated backgrounds from the Monte Carlo are too low in the electron sample and too high in the muon sample. A correction for these effects would change the estimated purities of identified semileptonic b-hadron decays by less than 2% relative.

The sensitivity of the average neutrino energy to the purity of the identified semileptonic decays has been studied using the subsample of semileptonic b-decay candidate events which are found in the lifetime tagged $b\bar{b}$ -sample IIa. This leads to a subsample of 1420 inclusive electron candidates and 2409 muon candidates. The purity for semileptonic b-hadron decays increases to 87% for the inclusive electron sample and to 76% for the inclusive muon sample. The predicted increase in the average neutrino energy for these subsamples of about 650 MeV with respect to the overall samples, is reproduced within 30 ± 230 MeV for the electron tagged events and 260 ± 180 MeV for the muon tagged events, where the errors are statistical only. As the relative energy sharing between the charged lepton and the neutrino is used to determine the underlying structure of the W^\pm polarization, the agreement between the charged lepton spectra in the data and the Monte Carlo is important. The b-hadron energy spectrum in the simulation has been simulated such that both the electron and the muon spectra are described simultaneously. The obtained agreement is not perfect as the average energy for detected electron candidates in the data is 100 ± 110 MeV lower than the corresponding one from the Monte Carlo; for the muon candidates the average energy in the data is 200 ± 70 MeV higher than the one in the Monte Carlo. The uncertainties in the prediction from the background corresponding to a change of about 50 MeV have already been taken into account. As the agreement for the average charged lepton energy is not perfect, an additional systematic error of ± 100 MeV due to momentum dependent efficiency uncertainties, is assumed for both the prediction of the average energy of the charged leptons and the neutrinos.

Adding the different error contributions in quadrature, the total systematic error on the average energy is 235 MeV for the ν_e candidates and 215 MeV for the ν_μ candidates. The individual contributions to the error are shown in Table 2.

| Error Source | $\Delta E(e^\pm)$ [MeV] | $\Delta E(\nu_e)$ [MeV] | $\Delta E(\mu^\pm)$ [MeV] | $\Delta E(\nu_\mu)$ [MeV] |
|--|-------------------------|-------------------------|---------------------------|---------------------------|
| Jet Energy Calibration | – | 150 | – | 150 |
| Purity of $b \rightarrow X\ell\nu \pm 5\%$ | 30 | 150 | 50 | 120 |
| ℓ^\pm Energy Uncertainty | 100 | 100 | 100 | 100 |
| Combined Error | 105 | 235 | 110 | 215 |

Table 2: The dominant contributions to the systematic error for the average charged lepton and neutrino energy measurement.

5 The Structure of the Weak Charged Current

Once the charged lepton spectra are described by a given model, the neutrino energy spectra are predicted. Therefore, a relative energy measurement of both the charged lepton and the neutrino allows the parity violation strength in semileptonic b -hadron decays to be determined. This can be done from a comparison of the average neutrino energy and the neutrino energy spectra in the data with different model predictions.

The accuracy in the measurement of the average neutrino energy mainly allows us the extreme assumptions of the free quark spectator model with a $(V-A) \times (V-A)$ or an exotic $(V+A) \times (V-A)$ decay structure possibility to be distinguished. The neutrino energy spectra for the $(V+A) \times (V-A)$ case have been obtained from a 4-vector Monte Carlo $(V+A) \times (V-A)$ simulation. This technique has been tuned by comparing a 4-vector $(V-A) \times (V-A)$ structure with the fully simulated events. The constraint that the average charged lepton energy remains constant is obtained with a harder b -fragmentation function, which increases the average b -hadron energy by about 7%. Using this procedure and correcting for background, the predicted average neutrino energies were found to be 900 ± 70 MeV larger for ν_e and 770 ± 60 MeV larger for ν_μ in the $(V+A) \times (V-A)$ simulation when compared to the $(V-A) \times (V-A)$ case.

The average energies for the charged leptons and the neutrinos in the data and the difference between the data and the Monte Carlo with a $(V-A) \times (V-A)$ and a $(V+A) \times (V-A)$ b -decay structure are given in Table 3. The measured average neutrino energy is found to be in good agreement with the $(V-A) \times (V-A)$ model and disagrees with the $(V+A) \times (V-A)$ model. Using the difference between the observed and predicted average neutrino energy, the $(V+A) \times (V-A)$ decay structure can be excluded with a significance of 3.8 standard deviations from the $b \rightarrow X e \nu_e$ candidates and with 2.5 standard deviations from the $b \rightarrow X \mu \nu_\mu$ candidates. Using alternatively the difference between the average energies of the charged lepton and the neutrino, the $(V+A) \times (V-A)$ structure can be excluded with a significance of about 3 standard deviations for each event sample. For a model with a kaon-like b -hadron decay structure with unpolarized virtual W^\pm 's the predicted average neutrino energy would be roughly 400 MeV larger than in

the $(V-A)\times(V-A)$ model. This possibility is disfavored by the data and can be excluded by more than 2 standard deviations if the two neutrino measurements are combined.

| type | particle | Data [GeV] | $(\langle E_\ell \rangle_{\text{Data}} - \langle E_\ell \rangle_{\text{MC}})$ [MeV] | |
|-------------------------------|-----------|--------------------------|---|--------------------------|
| | | $\langle E_\ell \rangle$ | $(V-A)\times(V-A)$ model | $(V+A)\times(V-A)$ model |
| $b \rightarrow X e \nu_e$ | electrons | 12.12 | $-100 \pm 110 \pm 105$ | $-100 \pm 110 \pm 105$ |
| $b \rightarrow X e \nu_e$ | neutrinos | 6.44 | $-120 \pm 120 \pm 235$ | $-1020 \pm 120 \pm 235$ |
| $b \rightarrow X \mu \nu_\mu$ | muons | 12.11 | $200 \pm 70 \pm 110$ | $200 \pm 70 \pm 110$ |
| $b \rightarrow X \mu \nu_\mu$ | neutrinos | 6.08 | $180 \pm 85 \pm 215$ | $-590 \pm 85 \pm 215$ |

Table 3: The measured average lepton energies $\langle E_\ell \rangle$ in the data and the difference between the data and the Monte Carlo for a $(V-A)\times(V-A)$ and a $(V+A)\times(V-A)$ b-decay model. The first error is the statistical error for the average energy values estimated from the r.m.s. of the distributions; the second error is the combined systematic error. The difference between average energies of the charged leptons in the $(V+A)\times(V-A)$ and the $(V-A)\times(V-A)$ model is constrained to be zero using a harder b-hadron fragmentation function for the $(V+A)\times(V-A)$ model.

In Figures 4a and b, the energy spectra of the ν_e and ν_μ candidates are compared with $(V+A)\times(V-A)$ and $(V-A)\times(V-A)$ simulations, using a Gaussian sigma of 4.2 GeV. A good description of the data is obtained for the $(V-A)\times(V-A)$ structure, while the $(V+A)\times(V-A)$ simulation shows a harder energy spectrum. To obtain a quantitative result from the spectrum, the numbers of observed neutrino events in four different energy regions have been compared with different model predictions. Large energy intervals were used to reduce the sensitivity to the systematic uncertainties in the accuracy of the neutrino energy measurement. The observed number of neutrino events per interval in the data and the difference between the number of data events and the ones expected by the different models are given in Table 4. The systematic errors have been obtained from a variation of the accuracy of the neutrino energy measurement, the accuracy was simulated with a Gaussian sigma of 4.2 ± 0.2 GeV; the relative purity error of $\pm 5\%$ and a possible energy scale shift between the data and the models of ± 200 MeV. The largest differences between the $(V-A)\times(V-A)$, $(V+A)\times(V-A)$ and the unpolarized $V\times(V-A)$ b-decay models are seen for the number of predicted high energy neutrinos. For low energies, the systematic errors due to the resolution of the measurement and the background contributions limit the possibility to discriminate between the models.

Taking only the number of observed events with neutrino energies above 16 GeV, the data are found to be in agreement with the $(V-A)\times(V-A)$ b-decay model and disagree with a significance of 5.7 and 3.7 standard deviations from the $(V+A)\times(V-A)$ model for the $b \rightarrow X e \nu_e$ and $b \rightarrow X \mu \nu_\mu$ candidates respectively. The obtained accuracy of this inclusive W^\pm polarization measurement is more significant than measurements of the parity violation strength in exclusive $B_{u,d} \rightarrow D^* \ell \nu$ decays [13]. Using the energy correlations between the charged lepton and the D^* meson, the CLEO collaboration has excluded a possible $(V+A)\times(V-A)$ b-decay structure with a significance of about 4 standard deviations.

The possibility of a b-decay model with a kaon-like $V\times(V-A)$ decay structure can be excluded by more than 3.5 standard deviations from the number of high energy neutrino events

for the $b \rightarrow X e \nu_e$ candidates. The neutrino energy spectrum from the $b \rightarrow X \mu \nu_\mu$ candidates is found to be equally consistent with the $(V-A) \times (V-A)$ and the $V \times (V-A)$ case.

| ν -energy range [GeV] | N_{Data} | $N_{\text{Data}} - N_{\text{MC}}$ | | |
|--|-------------------|-----------------------------------|----------------------|----------------------|
| | | $(V-A) \times (V-A)$ | $(V+A) \times (V-A)$ | $V \times (V-A)$ |
| $b \rightarrow X e \nu_e$ candidates | | | | |
| < 0.0 | 960 | $-27 \pm 39 \pm 47$ | $83 \pm 39 \pm 42$ | $42 \pm 39 \pm 44$ |
| 0.0–6.0 | 1782 | $11 \pm 53 \pm 101$ | $97 \pm 53 \pm 96$ | $39 \pm 53 \pm 99$ |
| 6.0–16.0 | 2106 | $58 \pm 58 \pm 107$ | $60 \pm 58 \pm 107$ | $60 \pm 58 \pm 107$ |
| > 16.0 | 518 | $-42 \pm 29 \pm 21$ | $-241 \pm 31 \pm 28$ | $-140 \pm 30 \pm 24$ |
| $b \rightarrow X \mu \nu_\mu$ candidates | | | | |
| < 0.0 | 1897 | $-76 \pm 55 \pm 119$ | $37 \pm 55 \pm 112$ | $-16 \pm 55 \pm 116$ |
| 0.0–6.0 | 3245 | $-132 \pm 71 \pm 78$ | $65 \pm 71 \pm 73$ | $-54 \pm 71 \pm 76$ |
| 6.0–16.0 | 3694 | $119 \pm 75 \pm 79$ | $152 \pm 75 \pm 78$ | $132 \pm 75 \pm 78$ |
| > 16.0 | 904 | $85 \pm 37 \pm 46$ | $-258 \pm 39 \pm 65$ | $-67 \pm 38 \pm 54$ |

Table 4: The observed number of events for different neutrino energy regions in the data and the difference between the data and the different models. The errors given for the difference include the estimated statistical and systematic errors due to background, energy scale and the assumed accuracy of the neutrino measurement.

We have also investigated if the measurement can be used to distinguish between the free quark model and exclusive b -decay models [14]. For these exclusive b -decay models the W^\pm polarization also depends on the spin of the produced hadron state. For example, the exclusive decays $B_{u,d,s} \rightarrow D_{u,d,s} \ell \nu$ are simulated with a $V \times (V-A)$ structure and show no polarization, while the majority of the other states are simulated with the $(V-A) \times (V-A)$ structure. The combination of the different decay modes was found to give essentially the same lepton spectra with at most a 50 MeV harder neutrino energy spectra when compared to the one obtained from the free quark model. Unfortunately, this difference is smaller than the accuracy of the measurement. The possibility that the expected large b -quark polarization is transferred to the b -baryon states² results in a small uncertainty for the predicted neutrino energy spectrum. Assuming that the b -quark polarization is completely transferred to the b -baryons, the predicted average neutrino energy would decrease by at most 80 MeV. Again, the difference is smaller than the accuracy of the measurement.

²Because of the long lifetime of b -hadrons, any possible primary b -quark polarization is lost for the spin 0 $B_{u,d,s}$ mesons.

6 Conclusions

The inclusive neutrino energy spectrum in semileptonic b-hadron decays has been measured from the missing energy of jets which contain energetic high p_t electron or muon candidates. The neutrino energy is measured with a resolution of about 4.2 GeV and an absolute energy scale accuracy of better than ± 150 MeV. Including the uncertainties due to the purity and the charged lepton spectra, the average neutrino energy is measured with a precision of ± 235 MeV in the electron and ± 215 MeV in the muon tagged b-hadron decays.

The observed number of neutrino candidates with energies above 16 GeV excludes b-hadron decay models with a $(V+A)\times(V-A)$ structure by more than 6 standard deviations and excludes the possibility that hadronic corrections to semileptonic b-hadron decays destroy any polarization of the virtual W^\pm by more than 3 standard deviations. In contrast to these exotic possibilities, the measured inclusive neutrino energy spectra are found to be in good agreement with the virtual W^\pm polarization expected from a $(V-A)\times(V-A)$ b-hadron decay structure.

For lower neutrino energies the systematic errors are found to be too large to draw definite conclusions. Nevertheless, using only the measurement of the average neutrino energy, models with a $(V-A)\times(V-A)$ b-decay structure are found to be in good agreement with the data, while the much larger average neutrino energy expected from a $(V+A)\times(V-A)$ b-hadron decay model can be excluded by about 4.5 standard deviations.

Acknowledgments

For several useful discussions we would like to thank Z. Was, E. Richter-Was and I. Bigi.

We also wish to express our gratitude to the CERN accelerator divisions for the excellent performance of the LEP machine. We acknowledge the contributions of all the engineers and technicians who participated in the construction and maintenance of this experiment.

The L3 Collaboration:

M. Acciarri,²⁶ A. Adam,⁴³ O. Adriani,¹⁶ M. Aguilar-Benitez,²⁵ S. Ahlen,¹⁰ J. Alcaraz,²⁵ A. Aloisio,²⁸ G. Alverson,¹¹ M.G. Alvigi,²⁸ G. Ambrosi,³³ Q. An,¹⁸ H. Anderhub,⁴⁶ A.L. Anderson,¹⁵ V.P. Andreev,³⁷ T. Angelescu,¹² L. Antonov,⁴⁰ D. Antreasyan,⁸ G. Alkhalov,³⁷ A. Arefiev,²⁷ T. Azemoon,³ T. Aziz,⁹ P.V.K.S. Baba,¹⁸ P. Bagnaia,^{36,17} J.A. Bakken,³⁵ L. Baksay,⁴² R.C. Ball,³ S. Banerjee,⁹ K. Banicz,⁴³ R. Barillere,¹⁷ L. Barone,³⁶ A. Baschiroto,²⁶ M. Basile,³ R. Battiston,³³ A. Bay,²² F. Becattini,¹⁶ U. Becker,¹⁵ F. Behner,⁴⁶ Gy.L. Bencze,¹³ J. Berdugo,²⁵ P. Berges,¹⁵ B. Bertucci,¹⁷ B.L. Betev,^{40,46} M. Biasini,³³ A. Biland,⁴⁶ G.M. Bilei,³³ R. Bizzarri,³⁶ J.J. Blaising,⁴ G.J. Bobbink,^{17,2} R. Bock,¹ A. Böhm,¹ B. Borgia,³⁶ A. Boucham,⁴ D. Bourilkov,⁴⁶ M. Bourquin,⁹ D. Boutigny,⁴ B. Bouwens,² E. Brambilla,¹⁵ J.G. Branson,³⁸ V. Brigljevic,⁴⁶ I.C. Brock,³⁴ M. Brooks,²³ A. Bujak,⁴³ J.D. Burger,¹⁵ W.J. Burger,¹⁹ C. Burgos,²⁵ J. Busenitz,⁴² A. Buytenhuijs,³⁰ A. Bykov,³⁷ X.D. Cai,¹⁸ M. Capell,¹⁵ G. Cara Romeo,⁸ M. Caria,³³ G. Carlini,²⁸ A.M. Cartacci,¹⁶ J. Casaus,²⁵ G. Castellini,¹⁶ R. Castello,²⁶ N. Cavallo,²⁸ M. Cerrada,²⁵ F. Cesaroni,³⁶ M. Chamizo,²⁵ Y.H. Chang,⁴⁸ U.K. Chaturvedi,¹⁸ M. Chemarin,²⁴ A. Chen,⁴⁸ C. Chen,⁶ G. Chen,⁶ G.M. Chen,⁶ H.F. Chen,²⁰ H.S. Chen,⁶ M. Chen,¹⁵ G. Chiefari,²⁸ C.Y. Chien,⁵ M.T. Choi,⁴¹ S. Chung,¹⁵ L. Cifarelli,⁸ F. Cindolo,⁸ C. Civinini,¹⁶ I. Clare,¹⁵ R. Clare,¹⁵ T.E. Coan,²³ H.O. Cohn,³¹ G. Coignet,⁴ N. Colino,¹⁷ V. Commichau,¹ S. Costantini,³⁶ F. Cotorobai,¹² B. de la Cruz,²⁵ X.T. Cui,¹⁸ X.Y. Cui,¹⁸ T.S. Dai,¹⁵ R.D. Alessandro,¹⁶ R. de Asmundis,²⁸ A. Degré,⁴ K. Deiters,⁴⁴ E. Dénes,¹³ P. Denes,³⁵ F. DeNotaristefani,³⁶ D. DiBitonto,⁴² M. Diemoz,³⁶ H.R. Dimitrov,⁴⁰ C. Dionisi,³⁶ M. Dittmar,⁴⁶ I. Dorne,⁴ M.T. Dova,^{18,4} E. Drago,²⁸ D. Duchesneau,¹⁷ F. Duhem,⁴ P. Duinker,¹ I. Duran,⁹ S. Dutta,⁹ S. Easo,³³ H. El Mamouni,²⁴ A. Engler,³⁴ F.J. Eppling,¹⁵ F.C. Erné,¹⁷ P. Extermann,¹⁷ R. Fabbretti,⁴⁴ M. Fabre,⁴⁴ S. Falciano,³⁶ A. Favara,¹⁶ J. Fay,²⁴ M. Felcini,⁴⁶ T. Ferguson,³⁴ D. Fernandez,²⁵ G. Fernandez,²⁵ F. Ferroni,³⁶ H. Fesefeldt,¹ E. Fiandrini,³³ J.H. Field,¹⁹ F. Filthaut,³⁰ P.H. Fisher,⁵ G. Forconi,¹⁵ L. Fredj,¹⁹ K. Freudenreich,⁴⁶ M. Gailloud,²² Yu. Galaktionov,^{27,15} E. Gallo,¹⁶ S.N. Ganguli,⁹ P. Garcia-Abia,²⁵ S.S. Gau,¹¹ S. Gentile,³⁶ J. Gerald,⁵ N. Gheordanescu,¹² S. Giagu,³⁶ S. Goldfarb,²² J. Goldstein,¹⁰ Z.F. Gong,²⁰ E. Gonzalez,²⁵ A. Gougas,⁵ D. Goujon,¹⁹ G. Gratta,³² M.W. Gruenewald,⁷ C. Gu,¹⁸ M. Guanzirol,¹⁸ V.K. Gupta,³⁵ A. Gurtu,⁹ H.R. Gustafson,³ L.J. Gutay,⁴³ B. Hartmann,¹ A. Hasan,²⁹ D. Hauschildt,² J.T. He,⁶ T. Hebbeker,⁷ M. Hebert,³⁸ A. Hervé,¹⁷ K. Hilgers,¹ H. Hofer,⁴⁶ H. Hoorani,¹⁹ S.R. Hou,⁴⁸ G. Hu,¹⁸ B. Ille,²⁴ M.M. Ilyas,¹⁸ V. Innocente,¹⁷ H. Janssen,⁴ B.N. Jin,⁶ L.W. Jones,³ P. de Jong,¹⁵ I. Josa-Mutuberria,²⁵ A. Kasser,²² R.A. Khan,¹⁸ Yu. Kamyshkov,³¹ P. Kapinos,⁴⁵ J.S. Kapustinsky,²³ Y. Karyotakis,¹⁷ M. Kaur,¹⁸ S. Khokhar,¹⁸ M.N. Kienzle-Focacci,¹⁹ D. Kim,⁵ J.K. Kim,⁴¹ S.C. Kim,⁴¹ Y.G. Kim,⁴¹ W.W. Kinnison,²³ A. Kirkby,³² D. Kirkby,³² J. Kirkby,¹⁷ S. Kirsch,⁴⁵ W. Kittel,³⁰ A. Klimentov,^{15,27} A.C. König,³⁰ E. Koffeman,² O. Kornadt,¹ V. Koutsenko,^{15,27} A. Koulbardi,³⁷ R.W. Kraemer,³⁴ T. Kramer,¹⁵ V.R. Krastev,^{40,33} W. Krenz,¹ H. Kuijten,³⁰ A. Kunin,^{15,27} P. Ladron de Guevara,^{25,17} G. Landi,¹⁶ S. Lanzano,^{28,1} P. Laurikainen,²¹ A. Lebedev,¹⁵ P. Lebrun,²⁴ P. Lecomte,⁴⁶ P. Lecoq,¹⁷ P. Le Coultre,⁴⁶ D.M. Lee,²³ J.S. Lee,⁴¹ K.Y. Lee,⁴¹ I. Leedom,¹¹ C. Legget,⁴ J.M. Le Goff,¹⁷ R. Leiste,⁴⁵ M. Lenti,¹⁶ E. Leonardi,³⁶ P. Levchenko,³⁷ C. Li,^{20,18} E. Lieb,⁴⁵ W.T. Lin,⁴⁸ F.L. Linde,²⁸ B. Lindemann,¹ L. Lista,²⁸ Y. Liu,¹⁸ W. Lohmann,⁴⁵ E. Longo,³⁶ W. Lu,³² Y.S. Lu,⁶ K. Lübelmeyer,¹ C. Luci,³⁶ D. Luckey,¹⁵ L. Ludovici,³⁶ L. Luminari,³⁶ W. Lustermann,⁴⁴ W.G. Ma,²⁰ M. MacDermott,⁴⁶ M. Maity,⁹ L. Malgeri,³⁶ R. Malik,¹⁸ A. Malinin,²⁷ C. Mañá,²⁵ S. Mangla,⁹ M. Maolinbay,⁴⁶ P. Marchesini,⁴⁶ A. Marin,¹⁰ J.P. Martin,²⁴ F. Marzano,³⁶ G.G. Massaro,² K. Mazumdar,⁹ T. McMahan,⁴³ D. McNally,³⁸ S. Mele,²⁸ M. Merk,³⁴ L. Merola,²⁸ M. Meschini,¹⁶ W.J. Metzger,³⁰ Y. Mi,²² A. Mihul,¹² G.B. Mills,²³ Y. Mir,¹⁸ G. Mirabelli,³⁶ J. Mnich,¹ M. Möller,¹ V. Monaco,³⁶ B. Montealeoni,¹⁶ R. Morand,⁴ S. Morganti,³⁶ N.E. Moulai,¹⁸ R. Mount,³² S. Müller,¹ E. Nagy,¹³ M. Napolitano,²⁸ F. Nessi-Tedaldi,⁴⁶ H. Newman,³² M.A. Niaz,¹⁸ A. Nippe,¹ H. Nowak,⁴⁵ G. Organtini,³⁶ R. Ostonen,²¹ D. Pandoulas,¹ S. Paoletti,³⁶ P. Paolucci,²⁸ G. Pascale,³⁶ G. Passaleva,^{16,33} S. Patricelli,²⁸ T. Paul,⁵ M. Pauluzzi,³³ C. Paus,¹ F. Pauss,⁴⁶ Y.J. Pei,¹ S. Pensotti,²⁶ D. Perret-Gallix,⁴ A. Pevsner,⁵ D. Piccolo,²⁸ M. Pieri,¹⁶ J.C. Pinto,³⁴ P.A. Piroué,³⁵ E. Pistolesi,¹⁶ F. Plasil,³¹ V. Plyaskin,²⁷ M. Pohl,⁴⁶ V. Pojidaev,^{27,16} H. Postema,¹⁵ N. Produit,¹⁹ J.M. Qian,³ K.N. Qureshi,¹⁸ R. Raghavan,⁹ G. Rahal-Callot,⁴⁶ P.G. Rancoita,²⁶ M. Rattaggi,²⁶ G. Raven,² P. Razis,²⁹ K. Read,³¹ M. Redaelli,²⁶ D. Ren,⁴⁶ Z. Ren,¹⁸ M. Rescigno,³⁶ S. Reucroft,¹¹ A. Ricker,¹ S. Riemann,⁴⁵ B.C. Riemers,⁴³ K. Riles,³ O. Rind,³ H.A. Rizvi,¹⁸ S. Ro,⁴¹ A. Robohm,⁴⁶ F.J. Rodriguez,²⁵ B.P. Roe,³ M. Röhner,¹ S. Röhner,¹ L. Romero,²⁵ S. Rosier-Lees,⁴ R. Rosmalen,³⁰ Ph. Rosset,²² W. van Rossum,² S. Roth,¹ J.A. Rubio,¹⁷ H. Rykaczewski,⁴⁶ J. Salicio,¹⁷ J.M. Salicio,²⁵ E. Sanchez,²⁵ G.S. Sanders,²³ A. Santocchia,³³ M.E. Sarakinos,³³ S. Sarkar,⁹ G. Sartorelli,¹⁸ M. Sassowsky,¹ G. Sauvage,⁴ C. Schäfer,¹ V. Schegelsky,³⁷ D. Schmitz,¹ P. Schmitz,¹ M. Schneegans,⁴ B. Schoenich,⁴⁵ N. Scholz,⁴⁶ H. Schopper,⁴⁷ D.J. Schotanus,³⁰ S. Shotkin,¹⁵ J. Shukla,²³ R. Schulte,¹ K. Schultze,¹ J. Schwenke,¹ G. Schwering,¹ C. Sciacca,²⁸ R. Sehgal,¹⁸ P.G. Seiler,⁴⁴ J.C. Sens,^{17,2} L. Servoli,³³ I. Sheer,³⁸ S. Shevchenko,³² X.R. Shi,³² E. Shumilov,²⁷ V. Shoutko,²⁷ D. Son,⁴¹ A. Sopczak,¹⁷ V. Soulimov,²⁸ C. Spartiotis,²¹ T. Spickermann,¹ P. Spillantini,¹⁶ M. Steuer,¹⁵ D.P. Stickland,³⁵ F. Sticozzi,¹⁵ H. Stone,³⁵ K. Strauch,¹⁴ K. Sudhakar,⁹ G. Sultanov,¹⁸ L.Z. Sun,^{20,18} G.F. Susinno,¹⁹ H. Suter,⁴⁶ J.D. Swain,¹⁸ A.A. Syed,³⁰ X.W. Tang,⁶ L. Taylor,¹¹ R. Timellini,⁸ Samuel C.C. Ting,¹⁵ S.M. Ting,¹⁵ O. Toker,³³ M. Tonutti,¹ S.C. Tonwar,⁹ J. Tóth,¹³ A. Tsaregorodtsev,³⁷ G. Tsiopolitis,³⁴ C. Tully,³⁵ H. Tuchscherer,⁴² J. Ulbricht,⁴⁶ L. Urbán,¹³ U. Uwer,¹ E. Valente,³⁶ R.T. Van de Walle,³⁰ I. Vetlitsky,²⁷ G. Viertel,⁴⁶ P. Vikas,¹⁸ U. Vikas,¹⁸ M. Vivargent,⁴ R. Voelkert,⁴⁵ H. Vogel,³⁴ H. Vogt,⁴⁵ I. Vorobiev,^{14,27} A.A. Vorobyov,³⁷ An.A. Vorobyov,³⁷ L. Vuilleumier,²² M. Wadhwa,²⁵ W. Wallraff,¹ J.C. Wang,¹⁵ X.L. Wang,²⁰ Y.F. Wang,¹⁵ Z.M. Wang,^{18,20} A. Weber,¹ R. Weill,²² C. Willmott,²⁵ F. Wittgenstein,¹⁷ D. Wright,³⁵ S.X. Wu,¹⁸ S. Wynhoff,¹ Z.Z. Xu,²⁰ B.Z. Yang,²⁰ C.G. Yang,⁶ G. Yang,¹⁸ X.Y. Yao,⁶ C.H. Ye,²⁰ J.B. Ye,²⁰ Q. Ye,¹⁸ S.C. Yeh,⁴⁸ J.M. You,¹⁸ N. Yunus,¹⁸ M. Yzerman,² C. Zaccardelli,³² P. Zemp,⁴⁶ M. Zeng,¹⁸ Y. Zeng,¹ D.H. Zhang,² Z.P. Zhang,^{20,18} B. Zhou,¹⁰ G.J. Zhou,⁶ J.F. Zhou,¹ R.Y. Zhu,³² A. Zichichi,^{8,17,18} B.C.C. van der Zwaan,²

-
- 1 I. Physikalisches Institut, RWTH, D-52056 Aachen, FRG[§]
 - III. Physikalisches Institut, RWTH, D-52056 Aachen, FRG[§]
 - 2 National Institute for High Energy Physics, NIKHEF, NL-1009 DB Amsterdam, The Netherlands
 - 3 University of Michigan, Ann Arbor, MI 48109, USA
 - 4 Laboratoire d'Annecy-le-Vieux de Physique des Particules, LAPP,IN2P3-CNRS, BP 110, F-74941 Annecy-le-Vieux CEDEX, France
 - 5 Johns Hopkins University, Baltimore, MD 21218, USA
 - 6 Institute of High Energy Physics, IHEP, 100039 Beijing, China
 - 7 Humboldt University, D-10099 Berlin, FRG[§]
 - 8 INFN-Sezione di Bologna, I-40126 Bologna, Italy
 - 9 Tata Institute of Fundamental Research, Bombay 400 005, India
 - 10 Boston University, Boston, MA 02215, USA
 - 11 Northeastern University, Boston, MA 02115, USA
 - 12 Institute of Atomic Physics and University of Bucharest, R-76900 Bucharest, Romania
 - 13 Central Research Institute for Physics of the Hungarian Academy of Sciences, H-1525 Budapest 114, Hungary[†]
 - 14 Harvard University, Cambridge, MA 02139, USA
 - 15 Massachusetts Institute of Technology, Cambridge, MA 02139, USA
 - 16 INFN Sezione di Firenze and University of Florence, I-50125 Florence, Italy
 - 17 European Laboratory for Particle Physics, CERN, CH-1211 Geneva 23, Switzerland
 - 18 World Laboratory, FBLJA Project, CH-1211 Geneva 23, Switzerland
 - 19 University of Geneva, CH-1211 Geneva 4, Switzerland
 - 20 Chinese University of Science and Technology, USTC, Hefei, Anhui 230 029, China
 - 21 SEFT, Research Institute for High Energy Physics, P.O. Box 9, SF-00014 Helsinki, Finland
 - 22 University of Lausanne, CH-1015 Lausanne, Switzerland
 - 23 Los Alamos National Laboratory, Los Alamos, NM 87544, USA
 - 24 Institut de Physique Nucléaire de Lyon, IN2P3-CNRS, Université Claude Bernard, F-69622 Villeurbanne Cedex, France
 - 25 Centro de Investigaciones Energeticas, Medioambientales y Tecnológicas, CIEMAT, E-28040 Madrid, Spain
 - 26 INFN-Sezione di Milano, I-20133 Milan, Italy
 - 27 Institute of Theoretical and Experimental Physics, ITEP, Moscow, Russia
 - 28 INFN-Sezione di Napoli and University of Naples, I-80125 Naples, Italy
 - 29 Department of Natural Sciences, University of Cyprus, Nicosia, Cyprus
 - 30 University of Nymegen and NIKHEF, NL-6525 ED Nymegen, The Netherlands
 - 31 Oak Ridge National Laboratory, Oak Ridge, TN 37831, USA
 - 32 California Institute of Technology, Pasadena, CA 91125, USA
 - 33 INFN-Sezione di Perugia and Università Degli Studi di Perugia, I-06100 Perugia, Italy
 - 34 Carnegie Mellon University, Pittsburgh, PA 15213, USA
 - 35 Princeton University, Princeton, NJ 08544, USA
 - 36 INFN-Sezione di Roma and University of Rome, "La Sapienza", I-00185 Rome, Italy
 - 37 Nuclear Physics Institute, St. Petersburg, Russia
 - 38 University of California, San Diego, CA 92093, USA
 - 39 Dept. de Física de Partículas Elementales, Univ. de Santiago, E-15706 Santiago de Compostela, Spain
 - 40 Bulgarian Academy of Sciences, Institute of Mechatronics, BU-1113 Sofia, Bulgaria
 - 41 Center for High Energy Physics, Korea Advanced Inst. of Sciences and Technology, 305-701 Taejon, Republic of Korea
 - 42 University of Alabama, Tuscaloosa, AL 35486, USA
 - 43 Purdue University, West Lafayette, IN 47907, USA
 - 44 Paul Scherrer Institut, PSI, CH-5232 Villigen, Switzerland
 - 45 DESY-Institut für Hochenergiephysik, D-15738 Zeuthen, FRG
 - 46 Eidgenössische Technische Hochschule, ETH Zürich, CH-8093 Zürich, Switzerland
 - 47 University of Hamburg, 22761 Hamburg, FRG
 - 48 High Energy Physics Group, Taiwan, China
- § Supported by the German Bundesministerium für Forschung und Technologie
‡ Supported by the Hungarian OTKA fund under contract number 2970.
‡ Also supported by CONICET and Universidad Nacional de La Plata, CC 67, 1900 La Plata, Argentina
† Deceased.

References

- [1] See, for example, D. G. Cassel, *b* physics, Proceedings DPF 92 (World Scientific, Singapore 1992) Vol. 1, p. 213-231, and references therein.
- [2] G. Altarelli *et al.*, Nucl. Phys. **B208** (1982) 365.
- [3] M. Gronau and S. Wakaizumi, Phys. Rev. Lett. **68** (1992) 1814.
- [4] M. Dittmar and Z. Was, Phys. Lett. **B332** (1994) 168.
- [5] L3 Collaboration, B. Adeva *et al.*, Nucl. Inst. and Meth. **A289** (1990) 35; O. Adriani *et al.*, Phys. Rep. **236** (1993) 1.
- [6] L3 Collaboration, B. Adeva *et al.*, Z. Phys. **C51** (1991) 179.
- [7] T. Sjöstrand, Comput. Phys. Commun. **27** (1982) 243; and “PYTHIA 5.6 and JETSET 7.3: Physics and manual”, preprint CERN-TH.6488/92.
- [8] The L3 detector simulation is based on GEANT Version 3.14; see R. Brun *et al.*, GEANT 3, CERN DD/EE/84-1 (Revised), September 1987 and the GHEISHA program (H. Fesefeld, RWTH Aachen Report PITHA85/02 (1985)) for the simulation of hadronic interactions.
- [9] Particle Data Group, L. Montanet *et al.*, Phys. Rev. **D50** (1994) 1173.
- [10] DELCO Collaboration, W. Bacino *et al.*, Phys. Rev. Lett. **43** (1979) 1073 and MARK III Collaboration, R. M. Baltrusaitis *et al.*, Phys. Rev. Lett. **54** (1985) 1976.
- [11] ARGUS Collaboration, H. Albrecht *et al.*, Phys. Lett. **B318** (1993) 397; see also CLEO Collaboration J. Gronberg *et al.*, CLEO Conf 94-6.
- [12] C. Peterson *et al.*, Phys. Rev. **D27** (1983) 105.
- [13] CLEO Collaboration, S. Sanghera *et al.*, Phys. Rev. **D47** (1993) 791 and ARGUS Collaboration, H. Albrecht *et al.*, Zeit. Phys. **C57** (1993) 533.
- [14] M. Wirbel, B. Stech and M. Bauer, Zeit. Phys. **C29** (1985) 637; N. Isgur, D. Scora, B. Grinstein and M. Wise, Phys. Rev. **D39** (1989) 799.

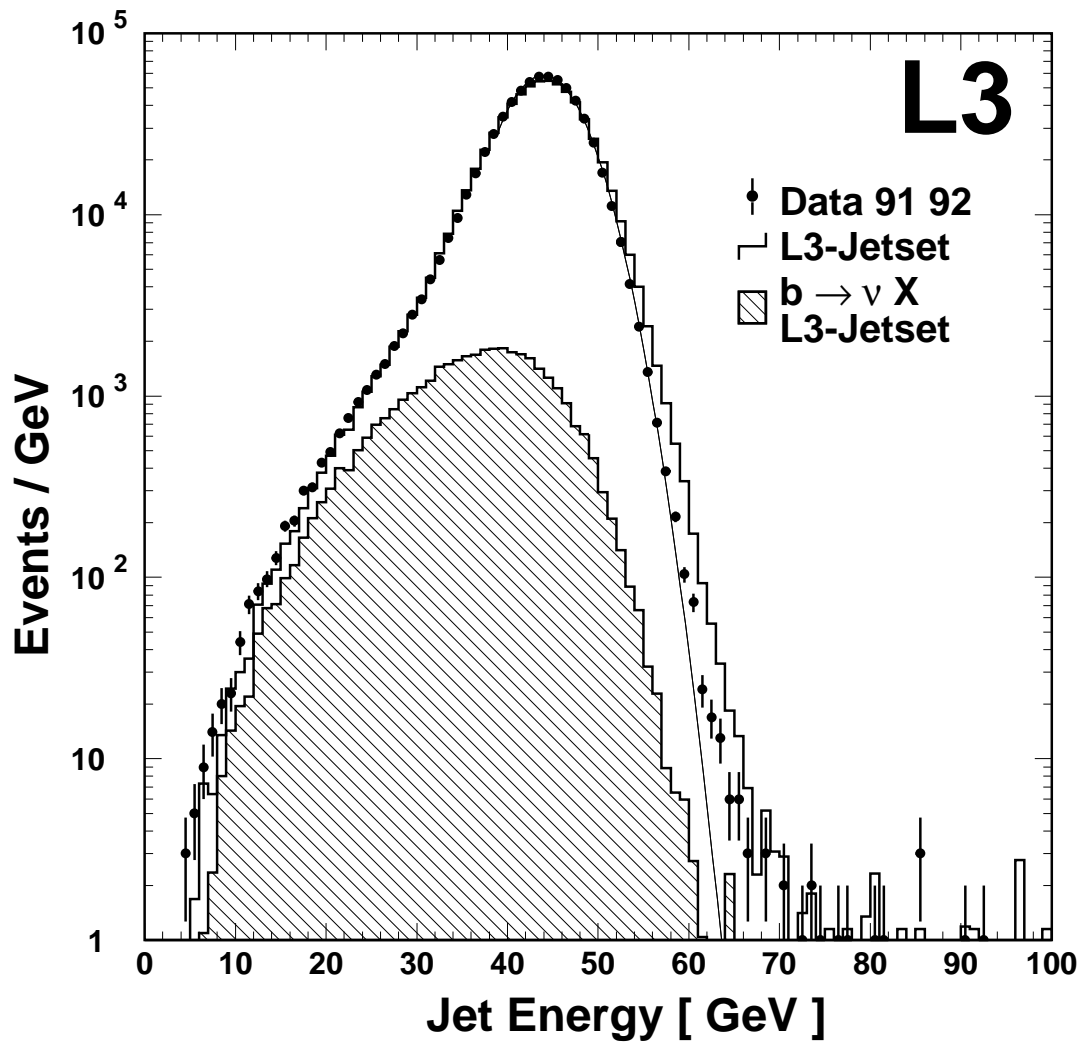


Figure 1: Visible energy per jet in the data and the Monte Carlo. The resulting curve from a Gaussian fit with a sigma of 4.2 GeV between 40 GeV and 65 GeV for the data is also shown; the sigma for the Monte Carlo is found to be 4.6 GeV. The expected jet energy distribution from semileptonic b-hadron decays is also shown.

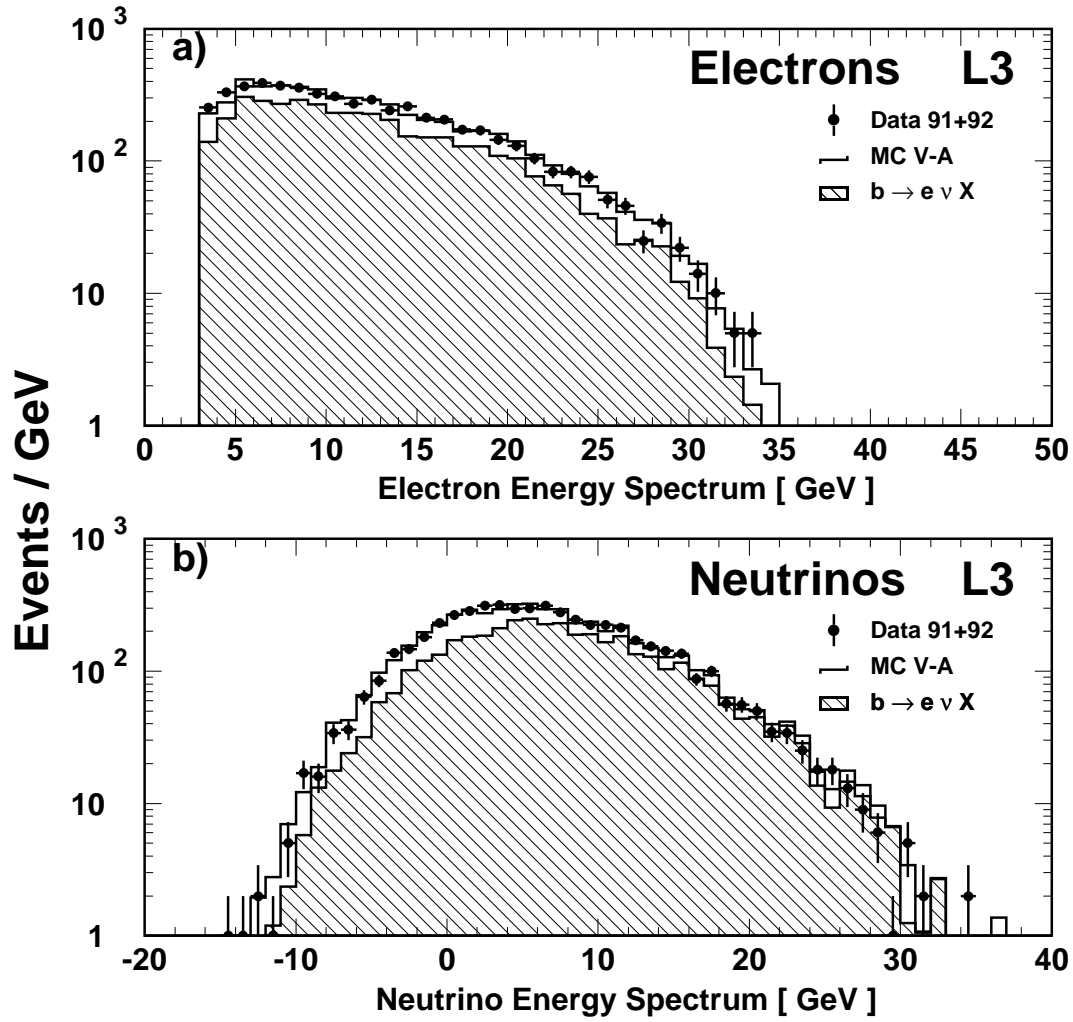


Figure 2: The energy spectrum of $b \rightarrow X e \nu$ candidates for (a) electrons and (b) neutrinos in the data and the $(V-A) \times (V-A)$ Monte Carlo. The estimated contribution from semileptonic b-hadron decays ($b \rightarrow X e \nu$) are also shown.

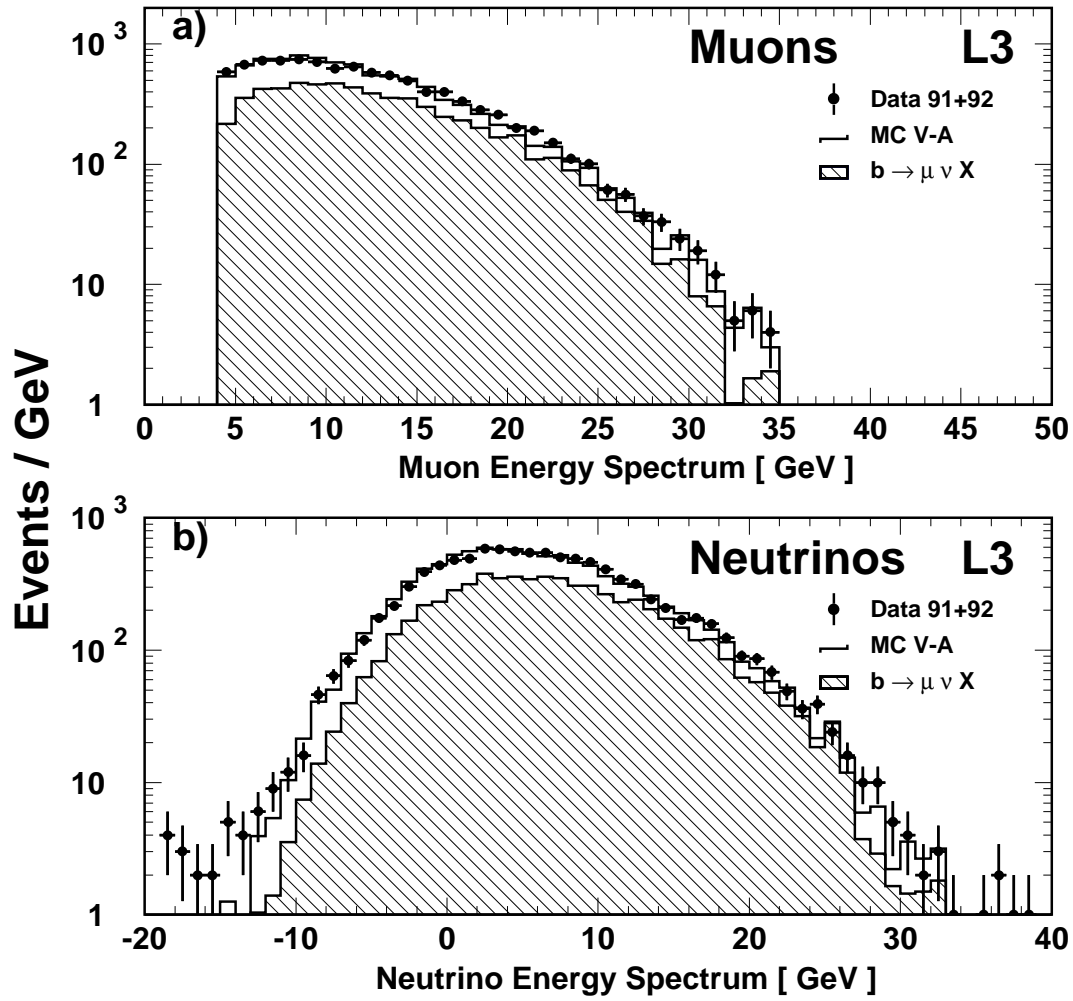


Figure 3: The energy spectrum of $b \rightarrow X \mu \nu$ candidates for (a) muons and (b) neutrinos in the data and the $(V-A) \times (V-A)$ Monte Carlo. The estimated contribution from semileptonic b -hadron decays ($b \rightarrow X \mu \nu$) are also shown.

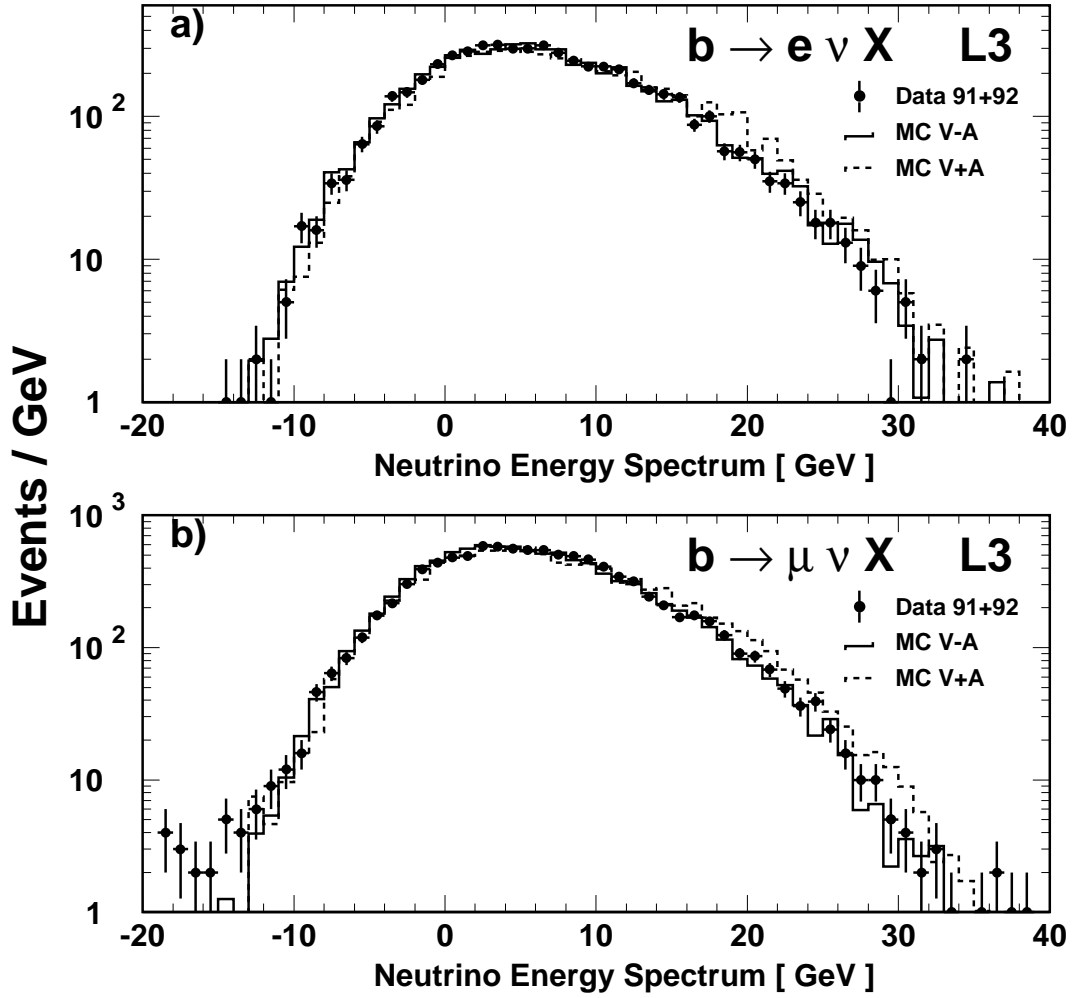


Figure 4: The missing energy spectrum of $b \rightarrow X \ell \nu$ candidates in the data and in the Monte Carlo with a $(V+A) \times (V-A)$ and a $(V-A) \times (V-A)$ b -hadron decay structure, (a) is for ν_e candidates and (b) for ν_μ candidates. The systematic uncertainties due the ν energy resolution and the background are not included.